

Supplementary Information

Alkali-Induced 3D Crinkled Porous Ti_3C_2 Mxene Architectures Coupled with NiCoP Bimetallic Phosphide Nanoparticles as Anodes for High-Performance Sodium-Ion Batteries

Experimental Section

Synthesis of 3D crinkled $\text{Ti}_3\text{C}_2\text{T}_x$ network

Ti_3AlC_2 powders (>98 wt % purity) were bought from Shanghai Vita Chemical Reagent Co., Ltd. 0.8 g LiF powders (Alfa Aesar, 98.5%) dissolved in 9 M HCl solutions (30 mL) and left under continuous stirring for 5 min, followed by the slow addition of Ti_3AlC_2 powders with a particle size of less than 38 μm (1 g) and heating of the mixture at 35 °C for 48 h. Then the solution was centrifuged at the speed of 3500 r and rinsed with deionized water several times till the pH of supernatant reached 6. The collection was dispersed into deionized water (100 ml) with ultrasonication treatment under bubbling Ar for 1 h, followed by centrifuging for 1 h at 3500 rpm. Finally the dark-green supernatant with few-layer $\text{Ti}_3\text{C}_2\text{T}_x$ flakes dispersed homogeneously was collected. The colloidal suspension (2 ml) was then mixed, at room temperature, with 1 M solutions of NaOH (2 ml). The $\text{Ti}_3\text{C}_2\text{T}_x$ nanosheets crumpled and flocculated rapidly accompanied by a mixture of solutions, and the suspension was rest for a few minutes. The flocculated deposit was separated from its solution by centrifugation. They were then washed with water one time and ethanol until neutral without shaking very strongly. The resulting materials were dried by freeze drying.

Synthesis of Ni-Co hydroxide precursors

For nickel/cobalt hydroxides, $\text{Ni}(\text{NO}_3)_2 \cdot 6\text{H}_2\text{O}$ (7.4 mg), $\text{Co}(\text{NO}_3)_2 \cdot 6\text{H}_2\text{O}$ (7.4 mg), and urea (2.25 g) were dissolved in a mixture of $\text{Ti}_3\text{C}_2\text{T}_x$ suspension (12.5 mL) and ethanediol (37.5 mL). Then, the solution was refluxed at 90 °C for 3 h in a flask under flowing Ar. The precipitate was centrifuged and washed with deionized water and alcohol for three times each after the flask was cooled down. Then the product was freeze-dried.

Synthesis of phosphides

A tube furnace with flowing Ar acting as the protective atmosphere was used for the phosphidation of the precursors. Two porcelain boats were used, one for the precursors and the other for NaH_2PO_2 . The porcelain boat for NaH_2PO_2 was located in the windward of the quartz tube. Then, the materials in the porcelain boats were calcined in Ar at 300 °C for 2 h with a heating rate of 2 °C min^{-1} . Black NiCoP powders were collected after naturally cooled down under flowing Ar.

Materials characterization

The crystal structure of the synthesized materials were carried out on a Rigaku D/Max-KA X-ray diffractometer equipped with a Cu K α source ($\lambda=1.5406 \text{ \AA}$) at a step size of 0.02° with 0.5 s dwelling time. The chemical content was estimated by thermogravimetric analysis (TGA) under a flow of N_2 atmosphere with a heating rate of 10 °C min^{-1} from RT to 600 °C. FTIR characterization was performed on Bruker spectrometer (SENSOR 27). Raman spectra were performed on a JY HR800 micro Raman spectrometer with a 633 nm laser as an excitation source. The exfoliated nanosheets were characterized using atomic force microscope (AFM, FM-Nanoview 1000). The morphologies, microstructure and elemental components of those materials were investigated by field emission scanning electron microscopy (FESEM, SU-70), and high-resolution transmission electron microscopy (HRTEM, JEM-2100) equipped with energy dispersive spectrometry (EDS) at an acceleration voltage of 200 kV, respectively.

Chemical compositions of the samples were further analyzed by high-resolution X-ray photoelectron spectroscopy (XPS) recorded with an ESCALAB 250 instrument equipped with a 150 W Al K α probe beam. Zeta potential measurements were performed with a Zetasizer Nano ZS apparatus from Malvern Instruments. Contact angles were measured on an OCA20 machine (Data-Physics, Germany) at room temperature.

Electrochemical measurements. To test electrochemical performance, the active materials, acetylene black (Super-P) and polyvinylidene fluoride binder were firstly mixed with the weight ratio of 70:20:10 and then dissolved in N-methyl-2-pyrrolidinone (NMP) to form homogenous slurry. The homogeneous slurry was coated onto Cu foil substrate and dried at 80 °C for 12 h. The mass loading of active materials in the working electrodes was about 1.0 mg. The obtained working electrodes were then assembled into 2025 coin-cells by using a sodium metal as reference electrode, glass fiber from Whatman as a separator and 1 M NaClO₄ in EC:DMC:EMC (1:1:1 wt%) with 5 wt% FEC additives as electrolyte. Galvanostatic charging/discharging (GCD) tests were performed on a LAND CT2001A instrument (Wuhan, China) with a potential range of 0.01-3.0 V at room temperature. Cyclic voltammetry (CV) curves between 0.01 and 3.0 V at a different scan rates and electrochemical impedance spectroscopy (EIS) with the frequency range between 100 KHz and 10.0 mHz were tested on an electrochemical workstation (PARSTAT2273).

Supplementary Figures

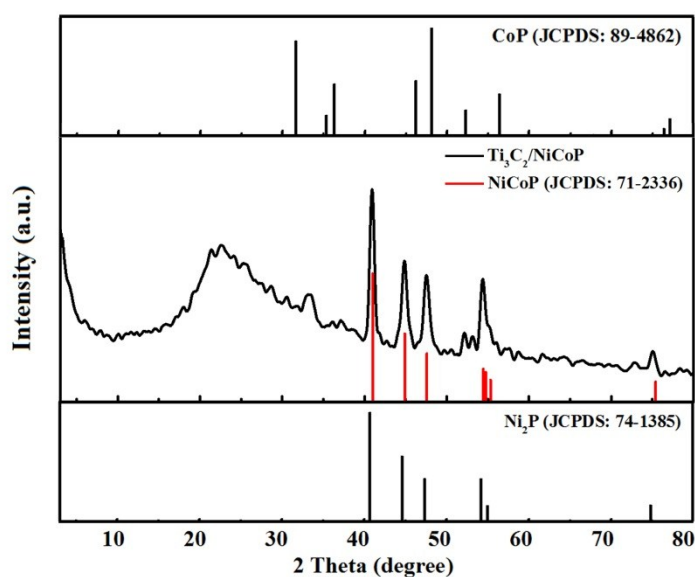


Figure S1. XRD patterns of Ti₃C₂/NiCoP, JCPDS of CoP, Ni₂P and NiCoP .

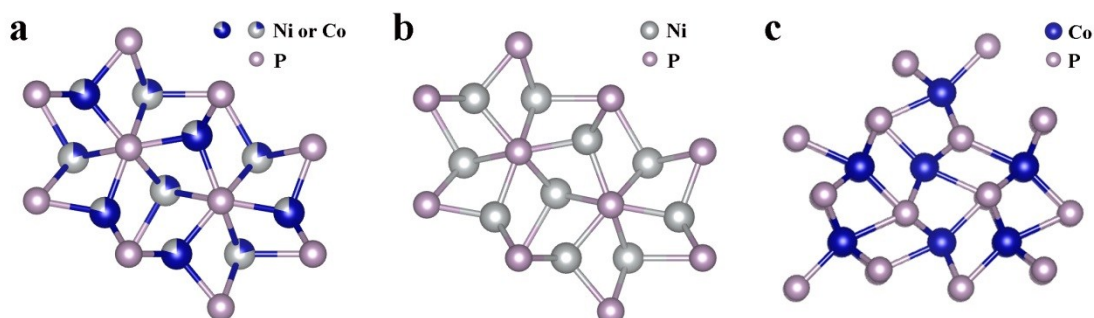


Figure S2. Schematic illustration of a) NiCoP (JCPDS No: 71-2336), b) Ni₂P (JCPDS No: 89-2742) and c) CoP (JCPDS No: 89-4862).

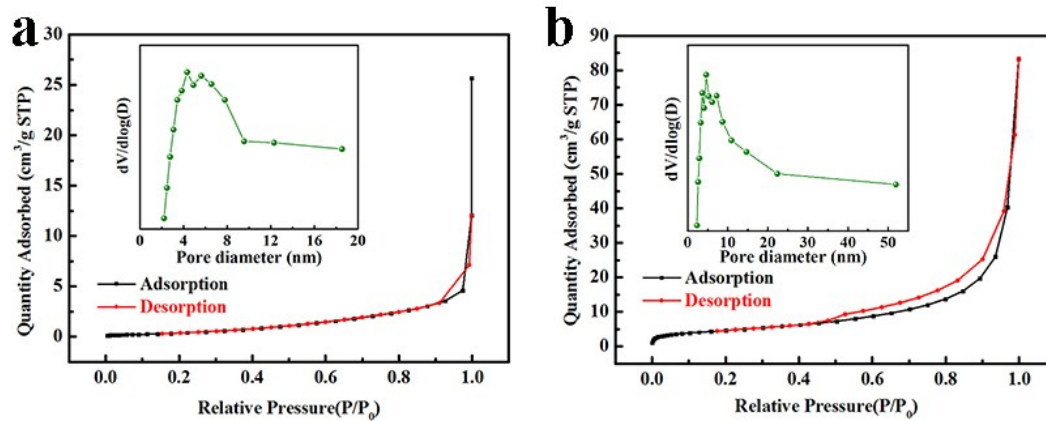


Figure S3. Nitrogen adsorption-desorption isotherm of a) Ti₃C₂ nanosheet and b) alkali-induced 3D Ti₃C₂ network. Insets are pore size distribution plot of samples.

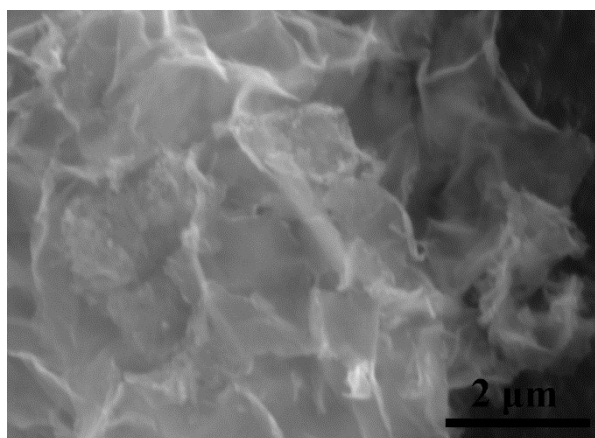


Figure S4. FESEM image of Ti₃C₂/NiCoP obtained by mechanical mixing, revealing inhomogeneous distribution of NiCoP nanoparticles on Ti₃C₂ nanosheet.

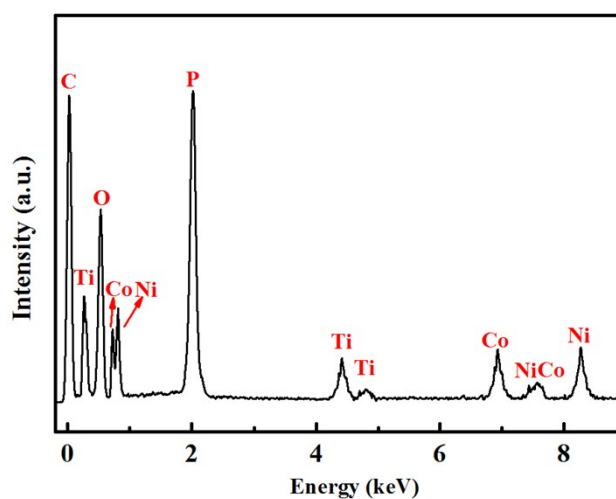


Figure S5. Energy dispersive X-ray spectroscopy (EDS) of Ti₃C₂/NiCoP composite.

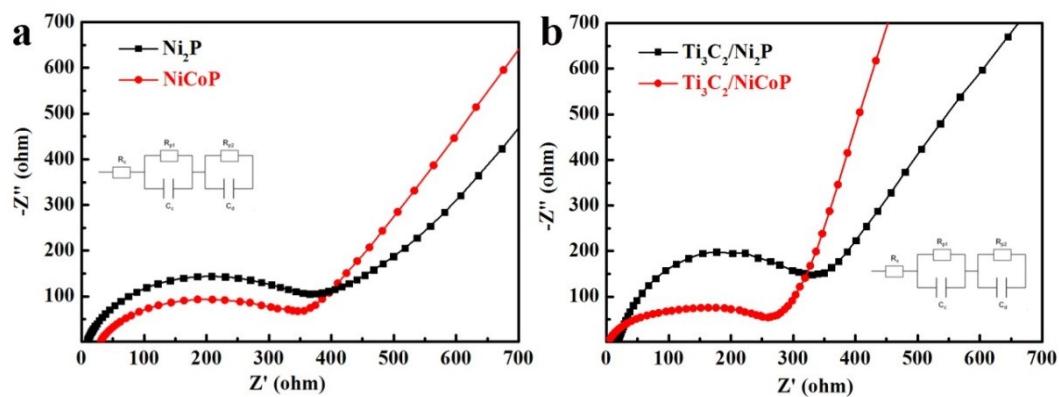


Figure S6. The EIS spectrum of Ni₂P (black) and NiCoP (red) (a) before and (b) after combination with Ti₃C₂.

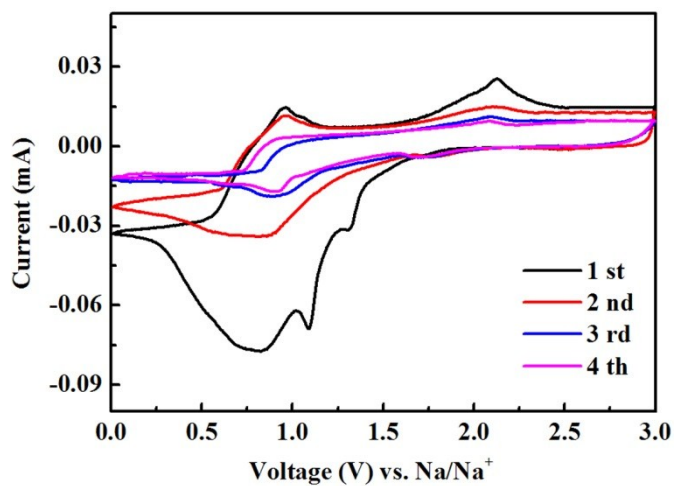


Figure S7. CV curves of pure NiCoP electrode at a scan rate of 0.1 mV s⁻¹.

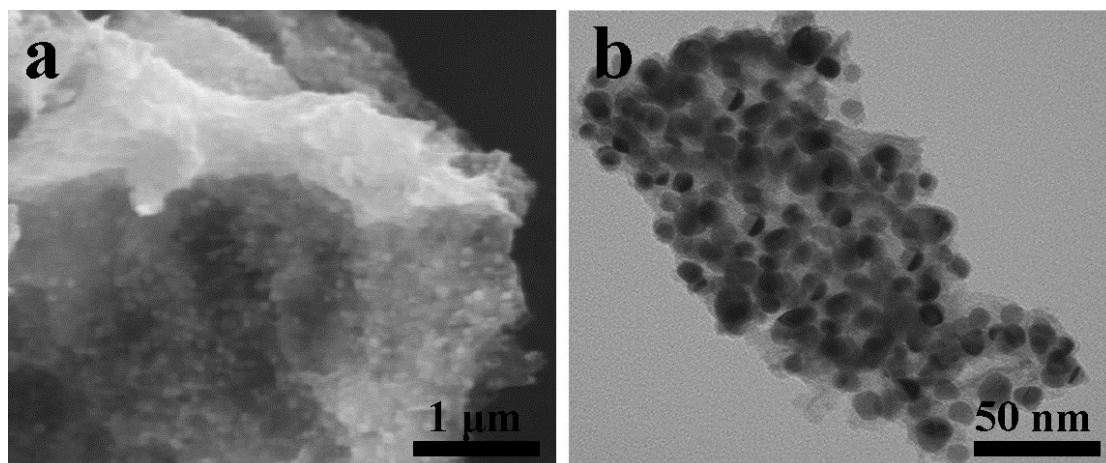


Figure S8. a) FESEM and b) low-magnification TEM images of Ti₃C₂/NiCoP electrode after 2000 cycles.

Table S1. Cycling performances comparison between present works with those of previously reported Ti_3C_2 -based and bimetallic phosphideSIBs anodes.

Electrode material	Voltage range (V)	Current density ($mA\ g^{-1}$)	Specific capacity ($mAh\ g^{-1}$)	Cycle number (N)	Ref [#]
f- $Ti_3C_2T_x$ -DMSO	0.01-2.5	1000	110	1500 cycles	1
Ti_3C_2 nanoribbon	0.01-3.0	200	191	150 cycles	2
Porous $Ti_3C_2T_x$	0.01-3.0	1000	189	1000 cycles	3
3D MXene sphere	0.01-3.0	500	295	1000 cycles	4
$Ni_{1.5}Co_{0.5}P_x/CNT$	0.01-3.0		188.9	100 cycles	5
This work	0.01-3.0	1000	261.7	2000 cycles	

References

1. Wu, Y.; Nie, P.; Wang, J.; Dou, H.; Zhang, X., Few-Layer MXenes Delaminated via High-Energy Mechanical Milling for Enhanced Sodium-Ion Batteries Performance. *ACS applied materials & interfaces* **2017**, *9* (45), 39610-39617.
2. Dong, Y.; Wu, Z.-S.; Zheng, S.; Wang, X.; Qin, J.; Wang, S.; Shi, X.; Bao, X., Ti_3C_2 MXene-derived sodium/potassium titanate nanoribbons for high-performance sodium/potassium ion batteries with enhanced capacities. *ACS nano* **2017**, *11* (5), 4792-4800.
3. Xie, X.; Kretschmer, K.; Anasori, B.; Sun, B.; Wang, G.; Gogotsi, Y., Porous $Ti_3C_2T_x$ MXene for Ultrahigh-Rate Sodium-Ion Storage with Long Cycle Life. *ACS Applied Nano Materials* **2018**, *1* (2), 505-511.
4. Zhao, M. Q.; Xie, X.; Ren, C. E.; Makaryan, T.; Anasori, B.; Wang, G.; Gogotsi, Y., Hollow MXene Spheres and 3D Macroporous MXene Frameworks for Na-Ion Storage. *Advanced materials* **2017**, *29* (37), 1702410.
5. Wang, X. W.; Guo, H. P.; Liang, J.; Zhang, J. F.; Zhang, B.; Wang, J. Z.; Luo, W. B.; Liu, H. K.; Dou, S. X., An Integrated Free-Standing Flexible Electrode with Holey-Structured 2D Bimetallic Phosphide Nanosheets for Sodium-Ion Batteries. *Advanced Functional Materials* **2018**, 1801016.